The structure and electronic state of photoexcited fullerene linked with a nitroxide radical based on an analysis of a two-dimensional electron paramagnetic resonance nutation spectrum

Norikazu Mizuochi, Yasunori Ohba, and Seigo Yamauchi
Institute for Chemical Reaction Science, Tohoku University, Katahira 2-1-1, Sendai 980-8577, Japan

(Received 29 December 1998; accepted 2 June 1999)

An electron paramagnetic resonance (EPR) study of 3,4-fulleropyrrolidine-2-spiro-4′-[2′,2′,6′,6′-tetramethyl]piperidine-1′-oxyl (**1**) was performed on the photoexcited quartet state in toluene glass. The spectrum of the $|S,Ms\rangle=|3/2,\pm 3/2\rangle\Leftrightarrow|3/2,\pm 1/2\rangle$ transitions was observed selectively by using a two-dimensional (2D) nutation method and analyzed with a spectral simulation in a randomly oriented system. A position of the nitroxide moiety was determined with respect to the zero-field splitting (zfs) axes of excited triplet fullerene ($^3C_{60}$) by taking into account of the dipolar–dipolar interaction between the radical and $^3C_{60}$, the hyperfine coupling, the anisotropic *g*-value of the nitroxide radical, and the zfs of the $^3C_{60}$ moiety. It was found that none of the zfs axes of the $^3C_{60}$ moiety coincide with the local C_2 axis of the molecule which is defined by the position of addition. A symmetry of the electronic structure in $^3C_{60}$ is discussed on the basis of the result. © *1999 American Institute of Physics.* [S0021-9606(99)01532-9]

I. INTRODUCTION

Fullerene (C_{60}) is a highly symmetric novel molecule having an icosahedral I_h symmetry in the ground state.[1,2] It is shown, however, by an electron paramagnetic resonance (EPR) technique that C_{60} distorts from the I_h symmetry in the photoexcited triplet state via an observation of zero-field splittings (zfs).[3,4] Although the molecular structure and the electronic state of the excited triplet states of C_{60} ($^3C_{60}$) have been extensively studied theoretically[5–7] and experimentally,[3,4,8–16] a description of the structure and even the symmetry of $^3C_{60}$ are still under the debate. On the basis of calculated energies and zfs of possible Jahn-Teller states having D_{5d}, D_{3d}, and D_{2h} symmetries, Surján *et al.* predicted that the state of D_{5d} symmetry is a little more stable (2 meV) than that of D_{2h} symmetry.[5–7] From an ODMR experiment,[12] the small *E*-value is observed ($D=-343.5$, $|E|=14.5$ MHz), which is not consistent with D_{5d} but rather consistent with the D_{2h} symmetry.

The zfs parameters of $^3C_{60}$ are considered to be very sensitive to modification of a molecular structure such as addition. From the x-ray structural analysis,[17] it is shown for monoadduct of C_{60} that the C_{60} moiety has a local C_2 axis which is parallel to a vector connecting a center of linked two carbons and a center of C_{60}. In several studies, [18,19] the structure[18] and reactivity[19] are discussed assuming that the molecule has the C_2 axis at that position even in the excited state. If the symmetry of the excited state is determined like those, the electronic structure of $^3C_{60}$ is expected to resemble closely that of $^3C_{60}$ under D_{2h}. However, the observed zfs of monoadduct fullerenes ($|D|=270-300$, $|E|=42-51$ MHz) (Refs. 20, 21) are much smaller than the calculated ones for the D_{2h} symmetry ($D=4.2\times10^2$, $|E|=1.2\times10^2$ MHz) (Ref. 7) and very similar to those for the D_{5d} symmetry ($D=-3.0\times10^2$, $E=0$ MHz).[7] These considerations indicate that more detailed experimental studies are needed to determine the electronic structure in the excited triplet state of monoadduct of C_{60}.

In this report we present a method to determine a relative position of addition of fullerene derivatives by using a radical probe. An analysis of magnetic interactions between the spins of photogenerated $^3C_{60}$ and the radical gives rise to information about the triplet spin distribution and the relative orientation of the nitroxide moiety with respect to the zfs axes of the $^3C_{60}$ moiety. In a previous study,[22] we reported a 2D EPR nutation study on radical linked to C_{60} **1** and confirmed that a photoexcited quartet state (Q_1) is generated in the radical–triplet ($R-T$) pair via the magnetic interaction.[23,24] Recently, Ishii *et al.* have reported an analysis of the quartet spectrum by spectral simulation,[25] where the principal axes of the *g*-matrix and the dipolar–dipolar tensor (D_{RT}) between the triplet and the radical are coaxial to that (D_T) of the triplet moiety. Here we report on the simulation of an EPR spectrum of the quartet state in a more general system where principal axes of *g*, hyperfine matrix, and D_{RT} are not coaxial to those of the zfs of the triplet moiety. The analysis is much more complicated than that in the coaxial system due to increased freedom of simulation parameters. In order to analyze a spectrum more straightforwardly and accurately, we use the 2D nutation method[22,26,27] and obtain the pure quartet spectrum which is separated from those of the other states.

To our best knowledge, this is the first report in which the relative orientation between the zfs axes of $^3C_{60}$ and the position of addition is determined.

II. EXPERIMENT

Compound **1** was synthesized by following the method of Corvaja *et al.*[24] and checked by fast atom bombardment

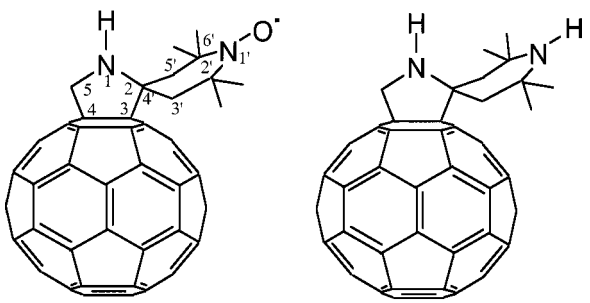

1 **2**

FIG. 1. Structures of 3,4-fulleropyrrolidine-2-spiro-4′-[2′,2′,6′,6′-tetramethyl]piperidine-1′-oxyl (**1**) and 3,4-fulleropyrrolidine-2-spiro-4′-[2′,2′,6′,6′-tetramethyl] piperidine (**2**).

mass (FAB-MS), UV-visible absorption, steady-state EPR, time-resolved (TR) EPR spectroscopy, and elementary analyses. 3,4-fulleropyrrolidine-2-spiro-4′-[2′,2′,6′,6′-tetrametyl] piperidine (compound **2**, Fig. 1) was newly synthesized in this study from 4-amino-4-carboxy-2,2,6,6,-tetrametylpiperidine (**3**, Scheme 1) and C_{60} by almost the same procedure as that of **1** (Scheme 1)

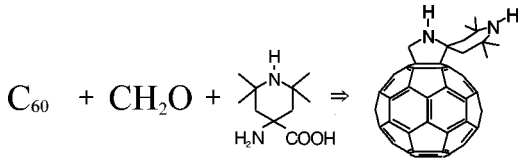

3 **2**

and checked by FAB-MS and UV-visible spectra.[28] Compound **3** was synthesized by following the literature.[29] C_{60} and **3** were removed from the reaction mixture by silica gel column chromatography and a middle fraction was used without further purification. For EPR measurements, the toluene solution (1×10^{-4} M) was deaerated by the freeze–pump–thaw method.

CW steady state EPR was measured on a Varian E-112 spectrometer using an Oxford ESR-9 helium gas flow system. The magnetic field was calibrated by using the perylene cation in conc. H_2SO_4 [$g=2.002\,569\pm0.000\,006$ (Ref. 30)] at room temperature.

CW-TREPR measurements were carried out at 10–80 K on a JEOL-FE2XG EPR spectrometer using an Oxford ESR 900 helium gas flow system. The samples were irradiated by the second harmonic (532 nm) of a Quanta-Ray GCR-230 Nd:YAG laser with a repetition rate of 10 Hz. Details of the TREPR measurement have been reported previously.[31]

2D nutation and electron-spin-echo (ESE) experiments were carried out at 5 K on a pulsed EPR spectrometer of our own design.[32,33] In the 2D nutation experiment the first microwave (MW) pulse of duration t_1 was applied at τ_d after a laser pulse of the second harmonic (532 nm) of a Continuum SL I-20 Nd:YAG laser with 20 Hz, where t_1 was incremented in 32 steps of 10 ns. A delay time τ_d was set to 20 ns to minimize effects of electron spin relaxation. A nutated magnetization was refocused by the second MW pulse with 110 ns in length and two-step phase cyclings [0,0]–[0,π] that is irradiated at 260 ns after the first MW pulse. An entire echo signal was integrated by an Evans gated integrator module Model 4130 with a sampling gate of 370 ns aperture. The pulse scheme is summarized in Fig. 2. An ESE-detected EPR spectrum was observed at each t_1 by plotting an intensity of accumulated ESE signals with respect to the magnetic field (B_0). Nutation signals, which were obtained as collected 2D ESE-detected EPR signals, were extrapolated to 100 points in t_1 dimension by the fast linear prediction procedure,[34,35] apodized with a cosine window and zero-filled to 1024 data points. 2D EPR nutation spectra were obtained from the Fourier-transformation of 2D ESE-detected EPR spectra in t_1 dimension.

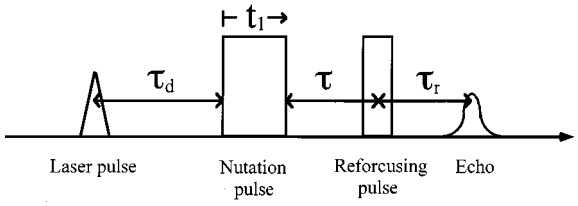

FIG. 2. A pulse sequence for the 2D nutation experiment. $\tau_d(=20$ ns) and $\tau(=260$ ns) are delay times between the laser pulse and the first microwave pulse and between the first and second microwave pulses, respectively. The spin packets are reforcused around τ_r after the second microwave pulse.

III. SIMULATION OF THE EPR SPECTRUM

A. Effective Hamiltonian and resonance field

The effective Hamiltonian of the quartet ($Q;S=3/2$) state in an interacting radical ($R;S=1/2$)-triplet ($T;S=1$) pair is given by[36]

$$H_Q=\beta\tilde{\mathbf{B}}\cdot\mathbf{g}\cdot\mathbf{S}+h\tilde{\mathbf{I}}\cdot\mathbf{A}\cdot\mathbf{S}+h\tilde{\mathbf{S}}\cdot\mathbf{D}_Q\cdot\mathbf{S}, \tag{1}$$

$$\mathbf{g}=\mathbf{g}_R/3+2\mathbf{g}_T/3, \tag{2}$$

$$\mathbf{D}_Q=\mathbf{D}_T/3+\mathbf{D}_{RT}/3, \tag{3}$$

$$\mathbf{A}=(1/3)\mathbf{A}_R\,. \tag{4}$$

Here $\sim$ denotes the transpose of a vector or a matrix, $\mathbf{D}_{RT}$ a dipolar–dipolar interaction tensor between R and T, $\mathbf{A}_R$ a hyperfine coupling matrix of a nitrogen nucleus of the nitroxide radical, and other symbols have usual meanings. $\mathbf{D}_T$, $\mathbf{g}_R$, $\mathbf{A}_R$, and $\mathbf{g}_T$ stand for those of a noncoupled radical or a triplet state. We neglected hyperfine couplings due to ^{13}C atoms on $^3C_{60}$, because the magnitude was estimated to be less than 1 MHz (Ref. 15) in the excited quartet states. Equations (2)–(4) are valid for the case, $|J|\gg|D|$,[37] which was ascertained by the 2D nutation method in this system.[22] In an analysis of the quartet spectrum, we use EPR parameters of the ground state of **1** and the excited triplet state of **2** for the radical and the triplet moieties of **1**, respectively.

Resonance fields are calculated by using the first order perturbation treatment[38] with the effective Hamiltonian given by Eq. (1). The Zeeman interaction is taken as the zeroth

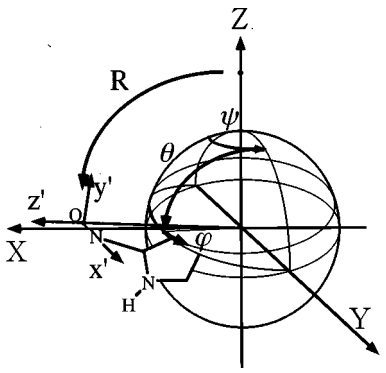

FIG. 3. The coordinate axis systems, *X, Y,* and *Z* denotes the zfs axes of the $^3C_{60}$ moiety. Angles θ, φ, and ψ are the Euler angles of rotation **R** (Ref. 37). $x'y'z'$ denote the axes of the nitroxide moiety.

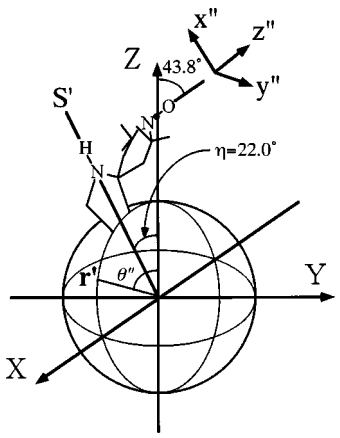

FIG. 4. Calculated angles obtained from the x-ray structural analysis (Ref. 17).

order term and the zfs and hyperfine interactions as the first order term. The resonance condition of the $|M_S,M_I\rangle \Leftrightarrow |M_S-1,M_I\rangle$ transition is expressed as

$$\nu = g\beta B/h + (3/2)\{\tilde{\mathbf{u}}\cdot\mathbf{D}_Q\cdot\mathbf{u}\}(2M_S-1) + KM_SM_I, \quad (5)$$

$$g^2 = \tilde{\mathbf{h}}\cdot\tilde{\mathbf{g}}\cdot\mathbf{g}\cdot\mathbf{h}, \quad (6)$$

$$\mathbf{u} = (\mathbf{g}\cdot\mathbf{h})/g, \quad (7)$$

$$K^2 = \tilde{\mathbf{u}}\cdot\tilde{\mathbf{A}}\cdot\mathbf{A}\cdot\mathbf{u}, \quad (8)$$

where **h** is a unit vector and parallel to the static magnetic field **B**. It is found from Eq. (5) that a zfs term is not involved for the $|S,Ms\rangle = |3/2,1/2\rangle \Leftrightarrow |3/2,-1/2\rangle$ transition in the first order ($2M_S$-1=0) but the zfs term including an interaction ($\mathbf{D}_{RT}$) between the radical and the triplet is included in the $|3/2,\pm 3/2\rangle \Leftrightarrow |3/2,\pm 1/2\rangle$ transitions.

The relative orientation of the nitroxide with respect to the zfs axes is defined by a set of the Euler angles θ, φ, and ψ (Ref. 39) as shown in Fig. 3 and described in Appendix A. The *X, Y,* and *Z* axes represent the zfs principal axes of the $^3C_{60}$ moiety and the x', y', and z' axes define the orientation of the nitroxide moiety where z' is directing from the center of C_{60} to the center of the N–O bond, y' axis is perpendicular to the pyrrolidine plane, and x' is orthogonal to z' and x'.

B. Dipolar interaction between radical and triplet C_{60}

The most important part of the simulation is an evaluation of the spin–spin interaction $\mathbf{D}'_{RT}$ between the radical and the triplet C_{60}. The smallest value of $|D_{RT}|$ in this system was calculated as ≈30 MHz under the simple point dipole approximation for the longest distance (12 Å) between the radical and two spins of $^3C_{60}$, where the triplet spins are localized at the opposite side of the C_{60} surface with respect to the radical. This calculation indicates that the contribution of D_{RT} is not negligible in comparison with $|D|$ of the triplet (**2**; 263 MHz).

We calculated the spin–spin interactions as a sum of the point dipolar–dipolar interactions between the single spin at the center of the N–O bond and a fraction of the triplet spins on a surface element on $^3C_{60}$ having a sphere of radius 3.5 Å. For a fraction of spins on a small surface element dS' with density ρ, a dipolar–dipolar interaction dD'_{RT} is expressed in the $x'y'z'$ coordinate system as

$$dD'_{RTii} = (1/2)(\mu_0/4\pi h)(g_e\beta)^2\rho((r'^2-3i^2)/r'^5)dS', \quad (i=x',y',z'), \quad (9)$$

$$dD'_{RTij} = (1/2)(\mu_0/4\pi h)(g_e\beta)^2\rho(-3ij/r'^5)dS', \quad (i=j=x',y',z'\, i\neq j). \quad (10)$$

Here μ_0 is the vacuum permeability and $\mathbf{r}'(x_r,y_r,z_r)$ is a vector connecting dS' and the center of the N–O bond as shown in Fig. 4. We neglected the *g* anisotropy and used the free electron *g*-value g_e in the calculation of $\mathbf{D}'_{RT}$. It should be noted that the dipolar–dipolar interaction between a triplet spin and a doublet spin is smaller by a factor of 2 as compared to that between a doublet spins. $\mathbf{D}'_{RT}$ is obtained by integrating dD'_{RT} in Eqs. (9) and (10) over the surface of C_{60} with the appropriate spin density distribution of the triplet. It is noted that there are two spins on $^3C_{60}$,

$$\int_{C_{60}\ \text{surface}} \rho dS' = 2. \quad (11)$$

The model of the spin distribution will be discussed in the later section. $\mathbf{D}'_{RT}$ is transformed into that in the *XYZ* system by the transformation matrix **R** in Appendix A.

C. Hyperfine coupling and *g* matrix of the radical

It is well known that the nitrogen hyperfine coupling and the *g* matrix of the nitroxides are almost coaxial and one of the principal axes lies along the N–O bond.[40] Here we describe these principal axes as x'', y'', and z'' as shown in Fig. 4. From the x-ray structural analyses of the nitroxide radical[41] and ground state C_{60},[17] the distance between the centers of C_{60} and the N–O bond is calculated as 8.24 Å, the angle η between the z' axis and the local C_2 axis (S') of **1** is 22.0° (Fig. 4). The angle between the N–O bond and the z' axis is calculated as 43.8°. $\mathbf{A}''_R$ and $\mathbf{g}''_R$ in the $x''y''z''$ axes

system are transformed to those of the *XYZ* system by the matrix **R** of rotation (Appendix A) as follows:

$$\mathbf{A}_R = \mathbf{R}^{-1}\mathbf{R}_{43.8}^{-1}\mathbf{A}_R''\mathbf{R}_{43.8}\mathbf{R}, \tag{12}$$

$$\mathbf{g}_R = \mathbf{R}^{-1}\mathbf{R}_{43.8}^{-1}\mathbf{g}_R''\mathbf{R}_{43.8}\mathbf{R}. \tag{13}$$

The transformation from the $x''y''z''$ system into the $x'y'z'$ system is made by rotation $\mathbf{R}_{43.8}$ with the Euler angles $\theta = 43.8°$, $\varphi = 0°$, and $\psi = 0°$.

D. Spin polarization

We evaluate the spin polarization of the quartet state in terms of initial spin polarizations of $^3C_{60}$ and the radical by using a density matrix formalism. The triplet density matrix ρ_T' in the zero-field and the doublet density matrix ρ_R in an infinite field are set to be both diagonal due to rapid relaxations of off-diagonal elements,[42–44]

$$\rho_T' = \begin{pmatrix} \rho_x & & \\ & \rho_y & \\ & & \rho_z \end{pmatrix} \begin{matrix} Tx \\ Ty, \\ Tz \end{matrix} \tag{14}$$

$$\rho_R = \begin{pmatrix} \rho_\alpha & \\ & \rho_\beta \end{pmatrix} \begin{matrix} \alpha \\ \beta. \end{matrix} \tag{15}$$

The elements of ρ_T' are determined by the rates of intersystem crossing from the excited singlet to the triplet sublevels in C_{60}. Any other spin polarizations are ignored and the spin polarizations of the quartet and doublet states are described by projections of ρ_T and ρ_R onto the coupled states.

ρ_T' in Eq. (14) is transformed into the finite field basis $|T_j\rangle$ $(j = 1,0-1)$ by a transformation matrix U_1,[45] which is described in Appendix B,

$$\rho_T = U_1^{-1}\rho_T' U_1. \tag{16}$$

The total density matrix of the triplet-radical pair is represented by a direct product of ρ_T and ρ_R,

$$\rho_{TD} = \rho_T \otimes \rho_R. \tag{17}$$

Here ρ_{TD} is expressed by a product basis $|1,m_s\rangle|1/2,m_s\rangle$ and transformed into the coupled basis as

$$\rho = U_2^{-1}\rho_{TD}U_2. \tag{18}$$

U_2 is a transformation from the product basis to the coupled basis and the matrix elements are described in Appendix B.

Only the diagonal elements of ρ are considered in a spectral simulation under an assumption of rapid relaxations of off-diagonal elements and the same validity holds as in Eq. (14).[42,44] Then the quartet spin polarization ρ_m $(m = 3/2,1/2,-1/2,-3/2)$ is calculated from the spin polarizations of the doublet ρ_k $(k = \alpha,\beta)$ and the triplet ρ_{T1} $(1 = 1,0,-1)$ as follows:

$$\rho_{3/2} = \rho_\alpha \rho_{T1}, \tag{19a}$$

$$\rho_{1/2} = (2/3)\rho_\alpha \rho_{T0} + (1/3)\rho_\beta \rho_{T1}, \tag{19b}$$

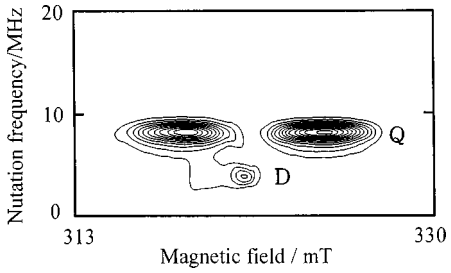

FIG. 5. A 2D nutation spectrum observed in toluene at 5 K. The microwave frequency is 9.030 GHz. The first microwave pulse was irradiated at 20 ns after the laser pulse.

$$\rho_{-1/2} = (1/3)\rho_\alpha \rho_{T-1} + (2/3)\rho_\beta \rho_{T0}, \tag{19c}$$

$$\rho_{-3/2} = \rho_\beta \rho_{T-1}. \tag{19d}$$

IV. RESULTS AND DISCUSSION

A. 2D EPR nutation spectrum

A two-dimensional (2D) EPR nutation spectrum of the photoexcited states of **1** was observed at 5 K as shown in Fig. 5. In the 2D spectrum, EPR signals are separated into two groups, *D* and *Q*, having different nutation frequencies, $\omega_D = 4.4$ MHz and $\omega_Q = 7.9$ MHz. In a previous report,[22] *D* and *Q* are assigned to the transition of the doublet state and the $|S,Ms\rangle = |3/2,\pm 3/2\rangle \Leftrightarrow |3/2,\pm 1/2\rangle$ transitions of the excited quartet state, respectively by using the equation,

$$\omega_n = \sqrt{S(S+1) - Ms(Ms-1)}\,\omega_1. \tag{20}$$

Here ω_n and ω_1 are nutation frequencies of a transition $|S,Ms-1\rangle \Leftrightarrow |S,Ms\rangle$ and of a system of $S = 1/2$, respectively. This relation is valid when *S* is a good quantum number and a transition is excited selectively by a microwave.[46] This method is very powerful to assign and separate spectra of a multiplet state.[22] In this case, the spectrum of the $|3/2, \pm 3/2\rangle \Leftrightarrow |3/2,\pm 1/2\rangle$ transitions was obtained by taking a slice of the 2D spectrum at $\omega_n = 7.9$ MHz.

B. EPR parameters of uncoupled triplet and doublet states

A TREPR spectrum of compound **2** in the triplet state was observed at 10 K and 0.5 μs after the laser excitation as shown in Fig. 6. The spectrum is simulated with zfs parameters and a populating ratio summarized in Table I, which are used in the simulation of the quartet spectrum. Obtained *D*- and *E*-values, $|D| = 263$ and $|E| = 39$ MHz, resemble closely not only those reported for other fullerene derivatives, $|D| = 270-300$ and $|E| = 42-51$ MHz,[20,21] but also those of $^3C_{60}$ in toluene ($|D| = 343.5$, $|E| = 14.5$ MHz).[12] From these results, it is considered that the spin distribution is almost the same among these fullerenes. Then, for the simulation of the quartet spectrum, we used the negative sign of *D*-value just same as that of $^3C_{60}$, which was determined from a pulsed ENDOR measurement on ^{13}C-enriched species by Groenen *et al.*[15] and also predicted from the theoretical studies.[6,7] For the spin density distribution, we adopted the model $\rho \propto \sin^2\theta''$ used in the ESEEM study.[16] Here θ'' denotes an

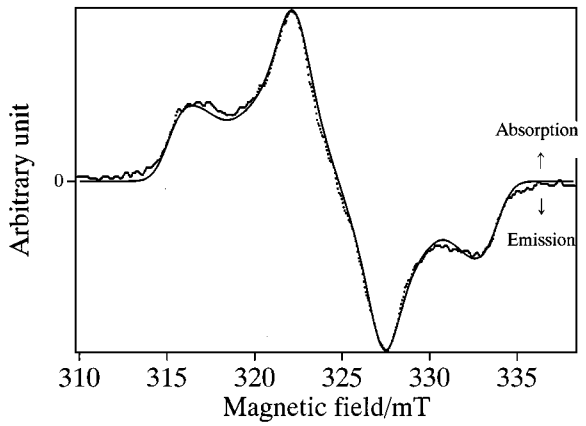

FIG. 6. A time-resolved EPR spectrum of the triplet state of **2** in toluene at 10 K and 0.5 μs after the laser excitation. The microwave frequency is 9.09176 GHz. Solid and dotted lines are simulated and observed spectrum, respectively.

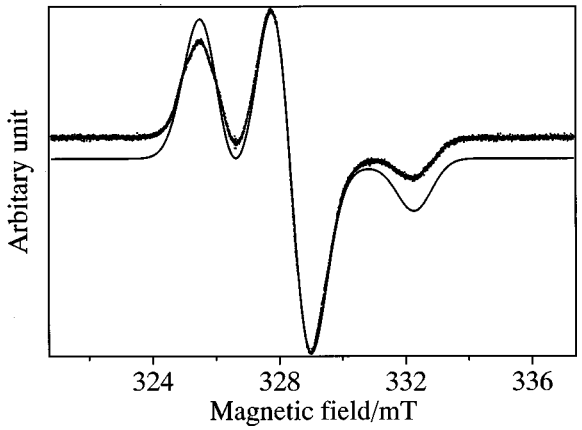

FIG. 7. An observed CW EPR spectrum of **1** in the ground state at 45 K (dots) and the simulated spectrum (line). The microwave frequency is 9.21754 GHz and an amplitude of 100 kHz field modulation is 1.25 G.

angle between the Z-axis of the zfs tensor of $^3C_{60}$ and a radius vector $\mathbf{r}'$ of the particular point on the surface of C_{60} (Fig. 4). This model is very simple but is appropriate enough to calculate the dipolar interaction in this system. The detailed dependence of the spin density distribution will be described in Sec. IV D.

It is well known that the rotational motion of C_{60} is not frozen even in a solid state[8,11,14] and an exchange of the zfs axes induces pseudorotational motions, resulting in averaged zero field interactions.[14] In contrast, monoadduct of fullerenes do not show such dynamical effects.[20] This is also a case of compound **2**, where the triplet spectrum does not show a temperature dependence from 5 K to 80 K. Therefore no dynamical effects are included in our calculation.

The g-values and the nitrogen hyperfine coupling constants are determined from those of the ground state of **1**. A conventional CW EPR spectrum of compound **1** observed at 45 K is shown in Fig. 7, which shows typical features of a nitroxide radical. From the simulation (Fig. 7), the g-values and the hyperfine coupling constants were obtained by assuming that those matrices were coaxial. The obtained parameters are summarized in Table I, where the values are fairly typical for nitroxide radicals. Although small uncertainties are included in the values, these affect least the simulated spectrum of the quartet state. The contributions of the g-value and the hyperfine interaction of the radical are reduced to a one-third in the quartet state as seen from Eqs. (2) and (4) and much smaller than that of $\mathbf{D}_Q$ as discussed in Sec. IV C.

TABLE I. The EPR parameters of **1** in the ground state and **2** in the photoexcited triplet state.

$g_{R_{x''x''}}=2.0022$[a]	$g_{R_{y''y''}}=2.0066$[a]	$g_{R_{z''z''}}=2.0101$[a]
$A_{R_{x''x''}}=92$ MHz[b]	$A_{R_{y''y''}}=14$ MHz[b]	$A_{R_{z''z''}}=14$ MHz[b]
$g_{TXX}=2.000$[c]	$g_{TYY}=2.000$[c]	$g_{TZZ}=2.001$[c]
$D_{TXX}=126$ MHz[d]	$D_{TYY}=49$ MHz[d]	$D_{TZZ}=-175$ MHz[d]
	$\lvert D_T\rvert=263$ MHz[d]	$\lvert E_T\rvert=39$ MHz[d]
Polarization	C_{60} radical	$(p_X-p_Z):(p_Y-p_Z)=0.45:1$
		$\rho_\alpha:\rho_\beta=0.54:0.47$

[a]The estimated error is ± 0.0005.
[b]The estimated error is ± 0.5 MHz. x'', y'', and z'' are the principal axes of the nitroxide radical.
[c]The estimated error is ± 0.001.
[d]The estimated error is ± 2 MHz. X, Y, and Z are the zfs principal axes of the $^3C_{60}$ moiety.

C. Zero field splittings and orientation of the nitroxide moiety

The Euler angles φ, θ, and ψ (Fig. 3) are used instead of spin Hamiltonian parameter D in order to reduce degrees of freedom in a spectral fitting procedure. We describe how a simulated spectrum depends on these parameters. It is important to note that spectral features are mostly determined by the zfs tensor $\mathbf{D}_Q$, where $\mathbf{D}_Q$ is dominated by φ and θ and does not depend on ψ. $\mathbf{D}_Q$ is a sum of two tensors, $\mathbf{D}_T/3$ and $\mathbf{D}_{RT}/3$ as described in Eq. (3). The former is assumed to be constant and the latter varies only with θ due to the cylindrical symmetry of the spin distribution ($\rho \propto \sin^2\theta'$). The calculated principal values of $\mathbf{D}_{RT}$ are summarized in Tables II and III for various θ values, where $\mathbf{D}_{RT}$ is almost axially symmetric and the magnitude is comparable with $\mathbf{D}_T$. As $\mathbf{D}_T$ is also almost axially symmetric, the resultant tensor $\mathbf{D}_Q$ mainly depends on an angle between the principal axes associated with the principle values of $\mathbf{D}_T$ and $\mathbf{D}_{RT}$ having the largest magnitude, which is approximately equal to θ in our case. Figure 8 shows the simulated spectra for various values

TABLE II. Principal values and direction cosines of $\mathbf{D}_{RT}$ and the zfs of the quartet state ($\mathbf{D}_Q$) with $\varphi=15°$, $\theta=65°$, $x=100°$.

Principal value		x[b]	y[b]	z[b]
$D_{RTx'''x'''}/3$[a]	26.9 MHz	0.895	−0.259	−0.364
$D_{RTy'''y'''}/3$[a]	29.1 MHz	0.238	0.996	−0.104
$D_{RTz'''z'''}/3$[a]	−56.0 MHz	0.379	6.8×10^{-3}	0.925
$D^a_{Q_{xx}}$	12.0 MHz	0.789	−0.407	0.461
$D^a_{Q_{yy}}$	46.0 MHz	0.380	0.912	0.154
$D^a_{Q_{zz}}$	−58.0 MHz	−0.483	0.0543	0.874

[a]The axes x''', y''', and z''' and x, y, and z denote the principal axes of $\mathbf{D}_{RT}$ and $\mathbf{D}_Q$, respectively.
[b]The direction cosines are referred to the zfs axes of $^3C_{60}$.

TABLE III. Principal values of $\mathbf{D}_{RT}$ and $\mathbf{D}_Q$ for typical orientations.

φ	θ	$D_{RTx'''x'''}/3$[a]	$D_{RTy'''y'''}/3$[a]	$D_{RTz'''z'''}/3$[a]	$D_{Qxx}/3$[a]	$D_{Qyy}/3$[a]	$D_{Qzz}/3$[a]
15°	65°	26.9	29.1	−56.0	12.0	46.0	−58.0
0°	0°	21.4	21.4	−42.8	37.8	63.4	−101.2
0°	45°	24.8	26.4	−51.2	38.5	41.1	−79.6
0°	90°	28.0	30.6	−58.6	−16.5	−27.9	44.4
0°	65°	26.9	29.1	−56.0	14.3	43.2	−57.5
30°	65°	26.9	29.1	−56.0	7.3	52.0	−59.3
45°	65°	26.9	29.1	−56.0	2.7	58.4	−61.1

[a]A MHz unit. The same axis systems are used as those of Tables I and II.

of θ. The separation of the lowest and the highest resonance fields, which corresponds to $4D_Q$ ($D_Q=-3/2D_{Qzz}$), strongly depends on θ.

Effects of φ on $\mathbf{D}_Q$ are rather complicated in comparison with those of θ and are shown in Fig. 9 around a region where the observed spectrum fits to the simulated one. In this region, φ mainly affects the rohmbicity of $\mathbf{D}_Q$ as also summarized in Table III.

The angle ψ provides relatively a small effect on the spectrum as shown in Fig. 10 around a region of the best fit parameters. The matrices of $\mathbf{g}_R$ and $\mathbf{A}_R$ were rotated around the z' axis.

D. Spectral simulation

The best fit simulation for the sliced spectrum of the $|S,Ms\rangle=|3/2,\pm 3/2\rangle\Leftrightarrow|3/2,\pm 1/2\rangle$ transitions is shown in Fig. 11. A set of the angles, $\varphi=15°\pm3°$, $\theta=65°\pm1°$, and $\psi=100°\pm10°$ were obtained. The principal values of $\mathbf{D}_Q$ and $\mathbf{D}_{RT}$ in the zfs axis system of $^3C_{60}$ are summarized in Table II. The other parameters obtained from the simulation are following: the distance r between radical and the center of C_{60} is 8.7 Å, which is consistent with the calculated value (8.24 Å) from the x-ray structural analysis of the nitroxide part. The linewidth is 0.9 mT as compatible with those of the ground state of **1** (1.1 mT) and the triplet state of **2** (1.4 mT). The doublet polarization were obtained as $\rho_\alpha=0.54$ and $\rho_\beta=0.47$.

As for the spin distribution, several models were examined in addition to the model $\rho\propto\sin^2\theta'$. For a model of the uniform distribution, the best fit angles were $\varphi=15°$, $\theta=67°$, and $\psi=100°$ and for the model $\rho\propto(\sin^2\theta'+\sin^4\theta'')$, where spins are concentrated more on the equator than that of the model $\rho\propto\sin^2\theta'$, the angles were $\varphi=15°$, $\theta=63°$, and $\psi=100°$. The observed spectra are reproduced well with these models and the obtained angles are not different so much in our system.

Small deviations between the observed and simulated spectra at the central part in Fig. 11 are considered to be due to the signal of the excited quartet $|3/2,1/2\rangle\Leftrightarrow|3/2,-1/2\rangle$ transition on the basis of the g-value and the spectral width.

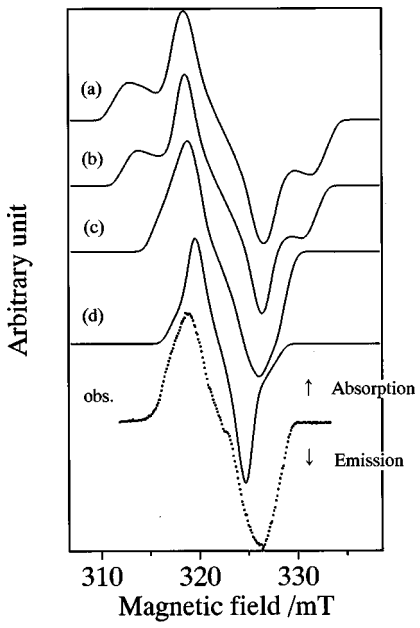

FIG. 8. An observed spectrum (dots) and simulated spectra (line) for various orientations of the nitroxide moiety with respect to the zfs axes of the $^3C_{60}$ moiety, (a) $\theta=0°$, (b) $\theta=30°$, (c) $\theta=60°$, and (d) $\theta=90°$. φ and ψ are set to zero. Other parameters used for the simulations are described in the text.

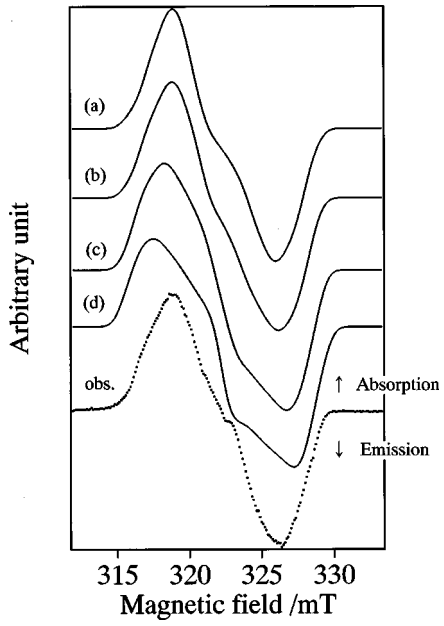

FIG. 9. An observed spectrum (dots) and simulated spectra (line) for various orientations of the nitroxide moiety with respect to the zfs axes of the $^3C_{60}$ moiety, (a) $\varphi=0°$, (b) $\varphi=15°$, (c) $\varphi=30°$, and (d) $\varphi=45°$. θ and ψ are set to 65° and 100°, respectively. Other parameters used for the simulations are described in the text.

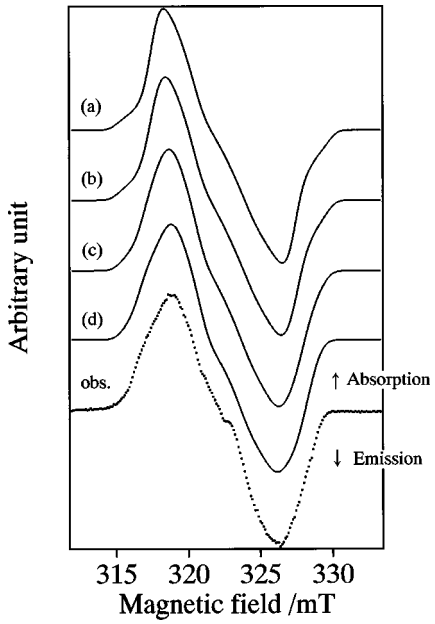

FIG. 10. An observed spectrum (dots) and simulated spectra (line) for the various orientation of the nitroxide moiety with respect to the zfs axes of $^3C_{60}$ moiety, (a) $\psi=0°$, (b) $\psi=30°$, (c) $\psi=60°$, and (d) $\psi=90°$. φ and θ are set to 15° and 65°, respectively. Other parameters used for the simulations are described in the text.

Although the nutation frequency of this transition is different from those of $|3/2,\pm 3/2\rangle \Leftrightarrow |3/2,\pm 1/2\rangle$, the separation of the spectra for these transitions was incomplete in the nutational frequency dimension because of a relatively large linewidth.

The observed spectrum shows a small asymmetry such that the absorptive signal at the lower field side is weaker than the emissive signal at the higher field side. In our static model, as we could not explain the reason of this asymmetry, we just set parameters ρ_α and ρ_β and obtained the ratio as $\rho_\alpha/\rho_\beta=1.2$ at 5 K. By comparing the integrated intensities between the observed and simulated spectra, it is found that ≈15% of the polarizations come from this asymmetric polarization and this value increases with raising temperature.

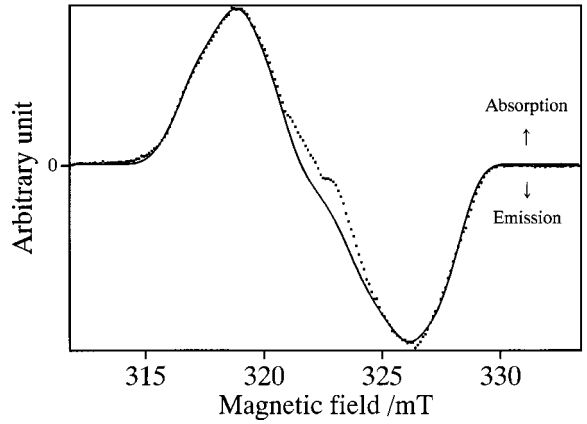

FIG. 11. An EPR spectrum of the $|S,Ms\rangle=|3/2,\pm 3/2\rangle \Leftrightarrow |3/2,\pm 1/2\rangle$ transitions obtained by slicing the 2D nutation spectrum at the frequency of 7.9 MHz (dots) and the simulated spectrum (line). Parameters used for the simulation are described in the text and Table I. The obtained angles are $\varphi=15°$, $\theta=65°$, and $\psi=100°$, respectively.

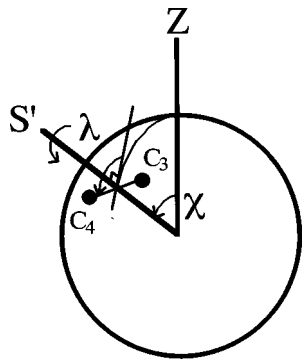

FIG. 12. Definition of the angles χ and λ. χ is an angle between Z and S' axes. λ is a rotation angle around S'. The C_3–C_4 bond lies in the ZS' plane for $\lambda=0°$.

In solution the radical triplet pair mechanism (RTPM) is proposed to be operative in this system.[24,47] However, it is not considered that this mechanism is involved in solid, because the RTPM does not provide any temperature dependent polarizations for a rigid molecule, where zfs D and the exchange interaction (J) between the excited doublet and quartet states are constants. It is also indicated from our nutation experiment that the spin quantum number is a good quantum number of the quartet state, which means the mixing between the quartet and doublet states is very small.[22] Analyses of the detailed temperature dependence of the EPR spectrum are in progress.

E. Position of addition and zfs axes of $^3C_{60}$

On the basis of the simulation, we discuss the position where the nitroxide moiety is linked to C_{60}. In order to represent the location of the position of addition, we introduce two angular parameters, χ and λ, as shown in Fig. 12, where S' is the local C_2 axis (Fig. 4) and χ is an angle between the S' and Z axes. The angle λ denotes a rotation of the C_3–C_4 bond around S' and the C_3–C_4 bond lies in the ZS' plane when $\lambda=0°$.

From the geometrical calculation, χ and λ were obtained as 63° and 89°, respectively. This result gives rise to a very important conclusion that the zfs axes of the $^3C_{60}$ moiety are far from the local C_2 axis and indicates that the local C_2 axis does not dominate the electronic structure of the $^3C_{60}$ moiety. If we refer to the fact that the mono-adduct and nonadduct of triplet fullerenes have similar zfs, the origin of the distortion is found to be the same for these fullerenes and namely the Jahn-Teller interaction.

In the excited triplet state, the symmetry of C_{60} is expected to be lowered to either D_{5d}, D_{2h}, or D_{3d} by the Jahn-Teller effect.[5–7] We examine the linked position by assuming that the Z axis of the zfs coincides with the symmetry axis of each distorted structure as shown in Fig. 13. For the three symmetries, the angles χ and λ which are closest to those of the simulation are calculated and summarized in Table IV together with the experimental result. The carbons of the selected C–C bond are indicated by the black-filled circles in Fig. 13. From the table it is found that the positions of the bounded carbons in D_{5d} realize the experimental re-

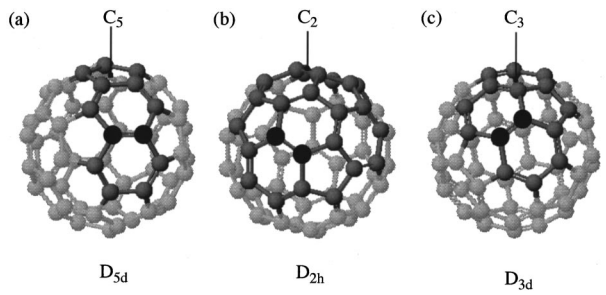

FIG. 13. Possible carbons for additions in the (a) D_{5d}, (b) D_{2h}, and (c) D_{3d} symmetries as indicated by black filled circles.

sult. Surján *et al.* showed that the triplet spin densities on the C_3 and C_4 carbons are very small in D_{5d},[7] which is consistent with the fact that *D*-values of $^3C_{60}$ and monoadduct of C_{60} are almost the same. It is also considered that the nitroxide moiety at this position hinders the pseudo-rotation of the zfs axes in contrast to the case of $^3C_{60}$.

Although many theoretical studies predict that the triplet state having D_{5d} symmetry is the most stable one among the possible Jahn-Teller states,[5–7] there are few experimental studies on the symmetry of $^3C_{60}$. As far as we know, only Bennati *et al.* reported the D_{5d} symmetry of $^3C_{60}$ from the analysis of the temperature dependence of the EPR line shape.[14] On the basis of our result and the similarity of the *D*-values of monoadduct of C_{60} and $^3C_{60}$, it is indicated that the electronic structure of $^3C_{60}$ belongs to the D_{5d} symmetry.

V. CONCLUSIONS

The 2D nutation spectrum of the quartet state of the $|S,Ms\rangle=|3/2,\pm 3/2\rangle \Leftrightarrow |3/2,\pm 1/2\rangle$ transitions was analyzed by the spectral simulation. The relative orientation between the zfs axes of the $^3C_{60}$ moiety and the nitroxide radical was determined. It is found that the zfs axis of C_{60} monoadduct in the triplet state is not parallel to the local C_2 axis which is originated from the position of addition. Therefore, the local C_2 axis does not dominate the electronic structure of the $^3C_{60}$ moiety in **1**. From the detailed examination of the linked position, it is indicated that the electronic structure of the $^3C_{60}$ moiety is close to the Jahn-Teller distorted D_{5d} structure. The similarity of the *D*-values of C_{60} monoadduct and $^3C_{60}$ is explained by the fact that $^3C_{60}$ also distorts to the structure of D_{5d} symmetry.

TABLE IV. Possible distorted structure.[a]

	Obs	D_{5d}	D_{2h}	D_{3d}
χ	63°	58°	72°	55°
λ	89°	90°	60°	150°

[a]See Fig. 13 for the definition of χ and λ.

ACKNOWLEDGMENTS

This work was supported by JSPS Research Fellowships for Young Scientists and a Grant-in-Aid for Scientific Research Nos. 07454145 and 08640630 from the Ministry of Education, Science, and Culture, Japan.

APPENDIX A

The relative orientation of the nitroxide with respect to the zfs axes is defined by a set of the Euler angles θ, φ, and ψ as shown in Fig. 3. Matrix **R** of the Euler rotation is represented as follows:

$$\mathbf{R}=\begin{pmatrix} \cos\psi\cos\varphi\cos\theta-\sin\psi\sin\varphi & \cos\psi\sin\varphi\cos\theta+\sin\psi\cos\varphi & -\cos\psi\sin\theta \\ -\sin\psi\cos\varphi\cos\theta-\cos\psi\sin\varphi & -\sin\psi\sin\varphi\cos\theta+\cos\psi\cos\varphi & \sin\psi\sin\theta \\ \cos\varphi\sin\theta & \sin\varphi\sin\theta & \cos\theta \end{pmatrix}. \tag{A1}$$

It is important to note that the *Z* axis crosses the center of the N–O bond when $\theta=\varphi=\psi=0°$.

APPENDIX B

U_1 is the transformation matrix between the zero field basis $|T_i\rangle$ $(i=x,y,z)$ and the finite field basis $|T_i\rangle$ $(j=1,0,-1)$ as the following:

$$|T_j\rangle=\sum_{i=x,y,z} U_{1,ij}|T_i\rangle, \tag{B1}$$

$$U_1=\begin{pmatrix} (-\cos\theta'\cos\phi'+i\sin\phi')/\sqrt{2} & \sin\theta'\cos\phi' & (\cos\theta'\cos\phi'+i\sin\phi')/\sqrt{2} \\ (-\cos\theta'\sin\phi'-i\cos\phi')/\sqrt{2} & \sin\theta'\sin\phi' & (\cos\theta'\sin\phi'-i\cos\phi')/\sqrt{2} \\ \sin\theta'/\sqrt{2} & \cos\theta' & -\sin\theta'/\sqrt{2} \end{pmatrix}, \tag{B2}$$

where θ' and ϕ' denote polar angles of an external magnetic field vector in the zfs principal axis system, B_0 $(\sin\theta'\cos\phi', \sin\theta'\sin\phi', \cos\theta')$.

U_2 is the transformation matrix between the product basis and the coupled basis as the following:

$$U_2 = \begin{array}{c} \\ Q_{3/2} \\ Q_{1/2} \\ Q_{-1/2} \\ Q_{-3/2} \\ D_{1/2} \\ D_{-1/2} \end{array} \begin{array}{c} \begin{array}{cccccc} T_1\alpha & T_0\alpha & T_{-1}\alpha & T_1\beta & T_0\beta & T_{-1}\beta \end{array} \\ \begin{pmatrix} 1 & 0 & 0 & 0 & 0 & 0 \\ 0 & \sqrt{2/3} & 0 & \sqrt{1/3} & 0 & 0 \\ 0 & 0 & \sqrt{1/3} & 0 & \sqrt{2/3} & 0 \\ 0 & 0 & 0 & 0 & 0 & 1 \\ 0 & -\sqrt{1/3} & 0 & \sqrt{2/3} & 0 & 0 \\ 0 & 0 & \sqrt{2/3} & 0 & -\sqrt{1/3} & 0 \end{pmatrix} \end{array}. \tag{B3}$$

[1] H. W. Kroto, J. R. Heath, S. C. O'Brien, R. F. Curl, and R. E. Smalley, Nature (London) **318**, 162 (1985).
[2] R. Taylor, J. P. Hare, A. K. Abdul-Sada, and H. W. Kroto, J. Chem. Soc. Chem. Commun. **20**, 1423 (1990).
[3] M. R. Wasielewski, M. P. O'Neil, K. R. Lykke, M. J. Pellin, and D. M. Gruen, J. Am. Chem. Soc. **113**, 2774 (1991).
[4] M. Terazima, N. Hirota, H. Shinohara, and Y. Saito, Chem. Phys. Lett. **195**, 333 (1992).
[5] P. R. Surján, L. Udvardi, and K. Németh, J. Mol. Struct.: THEOCHEM **311**, 55 (1994).
[6] P. R. Surján, K. Németh, M. Bennati, A. Grupp, and M. Mehring, Chem. Phys. Lett. **251**, 115 (1996).
[7] M. Kállay, K. Németh, and P. R. Surján, J. Phys. Chem. A **102**, 1261 (1998).
[8] G. L. Closs, P. Gautam, D. Zhang, P. J. Krusic, S. A. Hill, and E. Wasserman, J. Phys. Chem. **96**, 5228 (1992).
[9] E. J. J. Groenen, O. G. Poluektov, M. Matsushita, J. Schmidt, and J. H. van der Waals, Chem. Phys. Lett. **197**, 314 (1992).
[10] M. Bennati, A. Grupp, M. Mehring, K.-P. Dinse, and J. Fink, Chem. Phys. Lett. **200**, 440 (1992).
[11] A. Regev, D. Gamliel, V. Meiklyar, S. Michaeli, and H. Levanon, J. Phys. Chem. **97**, 3671 (1993).
[12] A. Angerhofer, J. U. V. Schütz, D. Widmann, W. H. Múller, H. U. T. Meer, and H. Sixl, Chem. Phys. Lett. **217**, 403 (1994).
[13] C. A. Steren, H. van Willigen, and K.-P. Dinse, J. Phys. Chem. **98**, 7464 (1994).
[14] M. Bennati, A. Grupp, and M. Mehring, J. Chem. Phys. **102**, 9457 (1995).
[15] G. J. B. van den Berg, D. J. van den Heuvel, O. G. Poluektov, I. Holleman, G. Meijer, and E. J. J. Groenen, J. Magn. Reson. **131**, 39 (1998).
[16] A. Grupp, J. Pfeuffer, and M. Mehring, *Physics and Chemistry of Fullerenes and Derivatives*, edited by H. Kuzmany, J. Fink, M. Mehring, and S. Roth (World Scientific, Singapore, 1995), p. 246.
[17] J. M. Hawkins, A. Meyer, T. A. Lewis, S. Loren, and F. J. Hollander, Science **252**, 312 (1991).
[18] (a) L. Pasimeni, A. Hirsch, I. Lamparth, A. Herzog, M. Maggini, M. Prato, C. Corvaja, and G. Scorrano, J. Am. Chem. Soc. **119**, 12896 (1997); (b) L. Pasimeni, A. Hirsch, I. Lamparth, M. Maggini, and M. Prato, *ibid.* **119**, 12902 (1997).
[19] A. Hirsch, I. Lamparth, and T. Grösser, J. Am. Chem. Soc. **116**, 9385 (1994).
[20] M. Bennati, A. Grupp, M. Mehring, P. Belik, A. Gügel, and K. Müllen, Chem. Phys. Lett. **240**, 622 (1995).
[21] (a) G. Agostini, C. Corvaja, M. Maggini, L. Pasimeni, and M. Prato, J. Phys. Chem. **100**, 13416 (1996); (b) L. Pasimeni, A. Hirsch, I. Lamparth, A. Herzog, M. Maggini, M. Prato, C. Corvaja, and G. Scorrano, J. Am. Chem. Soc. **119**, 12896 (1997).
[22] N. Mizuochi, Y. Ohba, and S. Yamauchi, J. Phys. Chem. A **101**, 5966 (1997).
[23] K. Ishii, J. Fujisawa, Y. Ohba, and S. Yamauchi, J. Am. Chem. Soc. **118**, 13079 (1996).
[24] C. Corvaja, M. Maggini, M. Prato, G. Scorrano, and M. Venzin, J. Am. Chem. Soc. **117**, 8857 (1995).
[25] K. Ishii, J. Fujisawa, A. Adachi, S. Yamauchi, and N. Kobayashi, J. Am. Chem. Soc. **120**, 3152 (1998).
[26] T. Takui, K. Sato, D. Shiomi, K. Itoh, T. Kaneko, E. Tsuchida, and H. Nishide, Mol. Cryst. Liq. Cryst. **279**, 155 (1996).
[27] A. V. Astashkin and A. Schweiger, Chem. Phys. Lett. **174**, 595 (1990).
[28] M. Maggini, G. Scorrano, and M. Prato, J. Am. Chem. Soc. **115**, 9798 (1993).
[29] A. Rassat and P. Rey, Bull. Soc. Chim. Fr. **815**, (1967).
[30] (a) B. G. Segal, M. Kaplan, and G. K. Fraenkel, J. Chem. Phys. **43**, 4191 (1965); (b) R. D. Allendoerfer, *ibid.* **55**, 3615 (1971).
[31] S. Ohkoshi, S. Yamauchi, Y. Ohba, and M. Iwaizumi, Chem. Phys. Lett. **224**, 313 (1994).
[32] Y. Ohba, N. Okabe, R. Satoh, K. Yamamoto, S. Yamauchi, and M. Iwaizumi, Appl. Magn. Reson. **6**, 51 (1994).
[33] Y. Ohba, R. Satoh, T. Kikuchi, S. Yamauchi, and M. Iwaizumi, J. Magn. Reson., Ser. A **103**, 282 (1993).
[34] C. F. Tirendi and J. F. Martin, J. Magn. Reson. **81**, 577 (1989).
[35] H. Gesmar and P. C. Hansen, J. Magn. Reson., Ser. A **106**, 236 (1994).
[36] A. Bencini and D. Gatteschi, *EPR of Exchange Coupled Systems* (Springer, Berlin, 1990).
[37] A. I. Shushin, Z. Phys. Chem. **182**, 9 (1993).
[38] M. Iwasaki, J. Magn. Reson. **16**, 417 (1974).
[39] M. E. Rose, *Elementary Theory of Angular Momentum* (Wiley, New York, 1957).
[40] *Biological Magnetic Resonance*, edited by L. J. Berliner and J. Reuben (Plenum, New York, 1989), Vol. 8.
[41] L. J. Berliner, Acta Crystallogr., Sect. B: Struct. Crystallogr. Cryst. Chem. **26**, 1198 (1970).
[42] U. E. Steiner and T. Ulrich, Chem. Rev. **89**, 51 (1989).
[43] C. C. Felix and S. I. Weissman, Proc. Natl. Acad. Sci. USA **72**, 4203 (1975).
[44] This assumption is generally used in a simulation of photoexcited triplet EPR spectra. If significant amounts of coherence exist, echolike responses may result after application of microwave pulses. The responses should decay with a phase memory time. Therefore, the validity can be confirmed by comparing the spectra of different laser delay times (τ_d). We compared the quartet EPR spectra of $\tau_d = 20$ ns with that of 1 μs and could not observe any significant differences.
[45] S. K. Wong, D. A. Hutchinson, and J. K. S. Wan, J. Chem. Phys. **58**, 985 (1973).
[46] A. Abragam, *The Principles of Nuclear Magnetism* (Clarendon, Oxford, 1961).
[47] C. Corvaja, M. Maggini, M. Ruzzi, G. Scorrano, and A. Toffoletti, Appl. Magn. Reson. **12**, 477 (1997).